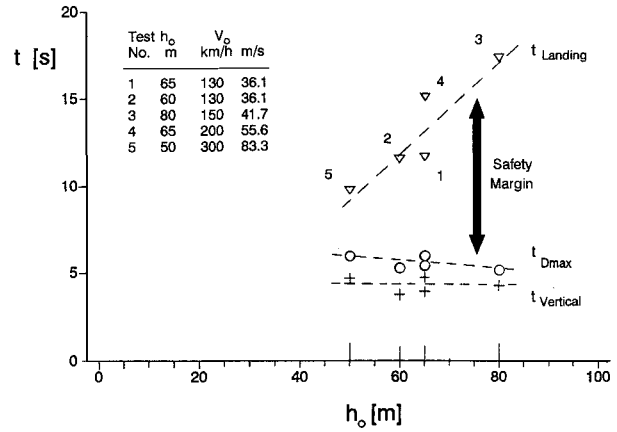

Fig. 3 Time sequences of the five drop tests.

cient can be calculated. Based on the constructive diameter D_c = 13.85 m:

$$C_{D_c} = \frac{mg}{(\rho/2)V_c^2(\pi/4)D_c^2} = 0.70$$

and, based on the nominal diameter D_0 = 11.81 m:

$$C_{D_0} = \frac{mg}{(\rho/2)V_c^2(\pi/4)D_0^2} = 0.96$$

With C_{D_c} = 0.70 the rate of descent of the reserve canopy will be about 6.0 m/s for a 100-kg payload and about 6.8 m/s for a 130-kg payload. This 9-m version of the LAP-LEONARDO is presently being investigated for its potential as a rescue parachute for glider, aircraft, and helicopter pilots.

Summary

A stable cross-type parachute of 13.85-m constructive diameter with an inflation aid for quick and reliable inflation has been developed as main canopy for low-altitude jumping from an aircraft or helicopter. A 9-m version of the so-called LAP-LEONARDO parachute has been designed as a reserve canopy and is also considered as a rescue parachute for pilots.

Acknowledgments

A number of dedicated parachute people like Peter Hoenen, Horst Buchsein, Norbert Frohwein, and Rüdiger Brumme, just to name some, designed, manufactured, and tested the parachute and financed the work.

References

[1]Hoenen, P., "Glider Recovery System," CCG-UofM-Course F12.01 on Parachute Systems Technology: Fundamentals, Concepts and Applications, Oberpfaffenhofen, Germany, June 1987.

[2]Krebber, B., "Rapidly Opening Parachute," CCG-UofM-Course F12.01 on Parachute Systems Technology: Fundamentals, Concepts and Applications, Oberpfaffenhofen, Germany, June 1987.

[3]Koch, R., "Technische Studie über Sprungfallschirmsysteme hoher Zuverlässigkeit für niedrige Absetzhöhen," DFVLR IB 154-73/4, Braunschweig, Germany, Nov. 1973.

[4]Fu, K.-H., and Koch, R., "Theoretical and Experimental Determination of Altitude Loss for Load-Systems Using Cluster Parachutes," AIAA Paper 75-1356, Nov. 1975.

[5]Johnson, D. W., and Peterson, C. W., "High-Speed, Low-Altitude Payload Delivery Using a Single Large Ribbon Parachute," AIAA Paper 84-0803, April 1984.

Forebody Vortex Control Using Nose-Boom Strakes

Limin Chen* and T. Terry Ng†
University of Toledo, Toledo, Ohio 43606
and
Brooke Smith‡
Eidetics International, Inc., Torrance, California 90505

I. Introduction

THE typical flowfield around a fighter-type aircraft at moderate-to-high angles of attack is dominated by vortices. The erratic behavior of these complex vortex flows at high angle of attack contribute to degraded control capability. The vortex-induced yawing moments are of sufficient magnitude that they often could not be overcome by the yawing moment generated by a deflected rudder. Many methods of controlling the forebody vortices have been developed recently, with some examples being Refs. 1–10.

One method of control is using small strakes located at or near the nosetip. The study by Ng and Malcolm[8] on a truncated F/A-18 forebody model showed that a rotatable strake on the nosetip is highly effective in controlling the forebody flow over a wide range of angles of attack and sideslip. The water tunnel study by Ng et al.[9] on an F-16 forebody model showed that miniature, rotatable strakes located on the nose boom are also effective in controlling the forebody vortices. In both cases, the positions of the forebody vortices can be controlled by rotating a strake to different roll angles relative to the nosetip. Significant control power can be obtained at angles of attack between 40–60 deg.

The objectives of the present experimental study are to determine the fluid mechanism of forebody vortex control using miniature, rotatable strakes at or near the nosetip, and to study aspects of the fluid mechanism that may be common to different forebody vortex control methods.

II. Experimental Setup

Two 1/10th-scale, F-16-like models were used. One is a full model tested at the NASA Langley Research Center 14- × 22-ft tunnel, and the other a forebody-only model tested at the University of Toledo 3- × 3-ft wind tunnel. The same forebodies were used in both tests. Force, moment, and surface pressure measurements were conducted at a tunnel dynamic pressure of 957.6 Pa (20 psf) for both tests. This corresponds to a Reynolds number of about 2.69 × 10^6/m (tunnel speed = 41.4 m/s). Additionally, smoke and surface flow visualizations were performed in the forebody-only test. The smoke flow visualization was conducted at a tunnel dynamic pressure of 47.9 Pa (1 psf), whereas the surface flow visualization was conducted at a tunnel dynamic pressure of 957.6 Pa (20 psf).

The forebody-only model was supported by a five-component (no axial force) force balance. A PSI electronic pressure scanner was set in the nose to measure the surface pressure distributions at fuselage stations 50 and 70. The full model tested was equipped with a six-component balance for measuring forces and moments, and three PSI electronic pressure

Received May 15, 1994; revision received Dec. 19, 1994; accepted for publication Dec. 27, 1994. Copyright © 1995 by the American Institute of Aeronautics and Astronautics, Inc. All rights reserved.

*Graduate Assistant, Department of Mechanical Engineering.
†Associate Professor, Department of Mechanical Engineering. Member AIAA.
‡Senior Engineer, Aeronautics Department.

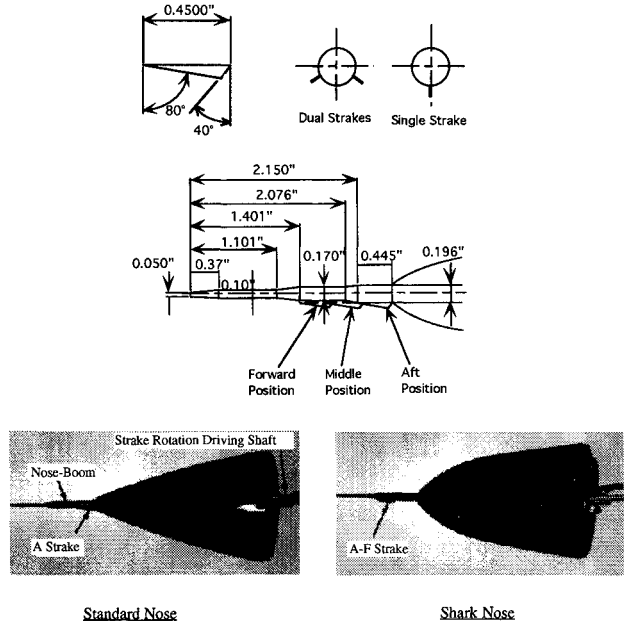

Fig. 1 Schematics of the forebody section of the model and the strakes.

scanners for pressure distributions at fuselage stations (FSs) 50, 70, 135, and 170.

Figure 1 shows schematics of the nose boom and the strakes. Variations to the strakes included: platform geometry, longitudinal position, and included angle for the dual strake configuration.[10] The baseline strake, designated as strake "A," was identified in previous water-tunnel[9] and wind-tunnel[10] investigations as the configuration with the best control characteristics. This strake has a leading-edge sweep of 80 deg, a trailing-edge of 40 deg (swept forward), and an exposed chord of 4.5-in. full-scale (0.45 in. at 1/10th-scale). The strake can be single or dual. The dual strake provides a better behaved control than the single strake.[9] It is, however, more convenient to study the fluid mechanism using the single strake due to the simpler geometry. The results to be presented will focus on the single strake. Three longitudinal strake positions, shown in Fig. 1, were tested. They are designated as A-fwd (A-F) strake, A-mid (AM) strake, and A-aft (A) strake, respectively.

Two kinds of nose geometry, shown in Fig. 1, were tested. They were called the standard F-16 nose and the shark nose. The shark nose has a larger platform area, a larger nose apex angle, and a higher cross-sectional AR than the standard nose.

Off-surface smoke flow visualizations were performed for the standard nose with strake A-fwd at an angle of attack of 50 deg. Laser sheet visualizations were performed at three different cross sections: 1-1, 2-2, and 3-3. Cross section 1-1 was located at the nosetip (Fuselage Station 0), cross section 2-2 at Fuselage Station 35, and cross section 3-3 at Fuselage Station 62.5.

III. Results

A. Yawing Moment Coefficient

Figure 2 shows the yawing moment coefficient variation with the strake roll angle at $\alpha = 50$ deg. The strake roll angle measures from the windward meridian in the counterclockwise direction from the pilot's view. The result of the standard nose illustrates that controlled yawing moments of different magnitudes can be obtained by rolling the strake to different angular positions. The yawing moment coefficient has a good linearity with the roll angle between approximately -45 and 45 deg.

The shark nose shows a smaller baseline asymmetry compared with the standard nose. The result again illustrates that

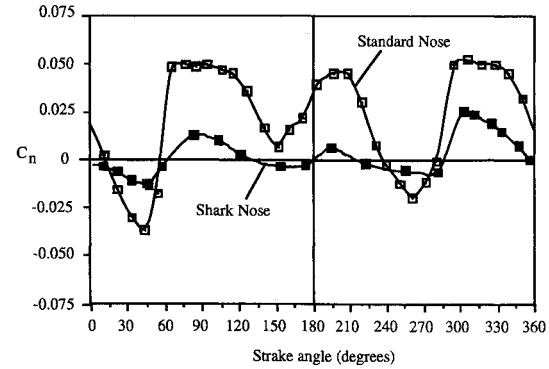

Fig. 2 Yawing moment coefficient variation with the strake roll angle for the standard and shark noses with strake A-fwd at an angle of attack 50 deg.

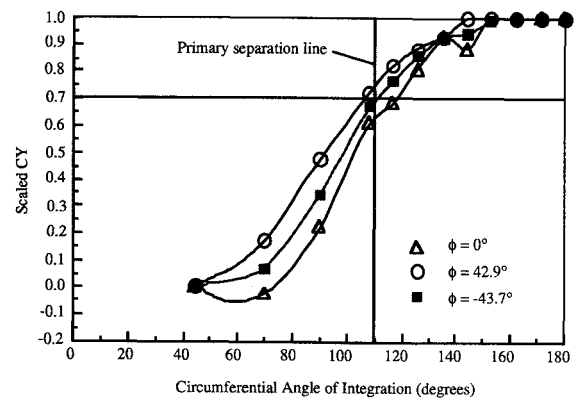

Fig. 3 Scaled sectional side force coefficient.

controlled yawing moments of different magnitudes can be obtained by rotating the strake to different angular positions. For the same strake, however, the yawing moments generated on the shark nose is smaller compared with the standard nose. The nose-boom strake nevertheless still has an appreciable control effect on the shark nose.

B. Surface Pressure Integral

The pressure changes extensively in both the primary and secondary flow regions as the strake rotates to different angular positions. The surface flow visualization and the pressure distribution results, however, indicate that the primary separation changes only slightly. To compare the contributions from different parts of the flow, a "sectional side force coefficient" (denoted as CY) is calculated as the integral of C_p along the surface between $\pm\phi$ as follows:

$$\mathrm{CY} = \int_{-\phi}^{\phi} C_p \frac{r\,d\phi}{D}$$

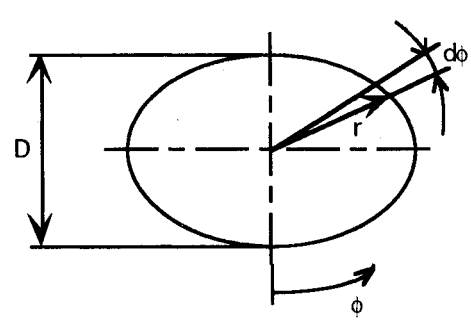

Figure 3 shows the sectional side force coefficients of the standard nose as a function of the circumferential angle of

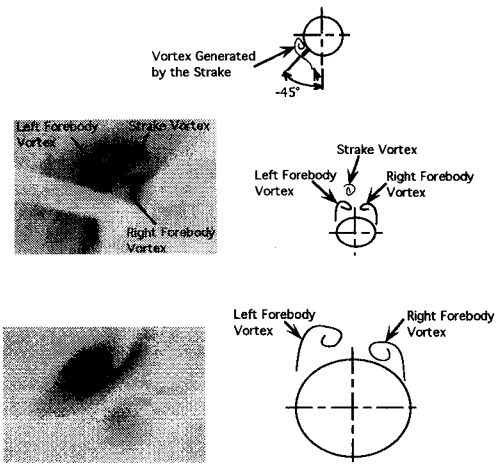

Fig. 4 Off-surface flow visualization for the standard nose with strake A-F at strake angle of −45 deg. Cross section a) 1-1 and b) 3-3.

integration. Results from three different strake roll angles at $\alpha = 50$ deg are shown. The sectional side force coefficients were scaled by their respective total CY (integrated between $\phi = \pm 180$ deg). The results illustrate that approximately 70% of the control power are from the region below the primary flow separation. The control power resulting from the leeward flow is relatively small. The yawing moment is thus generated mainly by asymmetric pressure distribution in the primary flow region. Similar results were obtained for the shark nose.

C. Flow Visualizations

Figure 4 shows the cross-sectional vortex flow patterns of the standard nose with strake A-fwd at a strake angle of −45 deg. At this position, the strake generates a vortex on the right side. At cross section 1-1, three vortices can be observed: one generated by the strake, and the other two are generated at the tip of the forebody. The resultant vortex positions are determined by the relative strengths of the vortices. The vortex from the A-fwd strake is situated farther from the surface than the forebody vortices. The strake vortex is also located closer to the right forebody vortex than the left one, and has the same sense of rotation as the right one. The right vortex is therefore "lifted" from the surface. At cross section 3-3, the asymmetry is amplified. The asymmetry in the forebody vortices is thus reversed from the baseline asymmetry that features a "high" left vortex.

At the strake angle of +45 deg, the strake generates a vortex on the left side. The effect is the opposite of that at $\phi = 45$ deg. The asymmetry in the forebody vortices is thus increased from the baseline asymmetry.

The surface flow visualizations illustrate that the secondary flow separation near the nose tip can be strongly affected by the strake vortex, and there is a strong correlation between the secondary pattern and the vortex asymmetry. The result also illustrates, however, that the primary flow separation lines change only slightly when the strake rotates to different angular positions.

IV. Conclusions

The method was shown to be effective in producing control yawing moments over a wide range of angles of attack. The strake function by acting as a vortex generator, and a vortex is an effective means of controlling other vortices. The strake generates vortices with different trajectories and strength as it rotates to different angular positions on the nose boom. The strake vortex interacts with the forebody vortices near the nosetip. The forebody vortices readjust their orientations due to the interaction. Different velocities and pressures are thereby induced on the two sides of the object by the asymmetric potential vortex flow. Controlled side forces and yawing moments of different magnitudes are therefore generated. The surface pressure integration shows that the side force is generated mostly in the primary flow region.

References

[1]Malcolm, G. N., and Skow, A. M., "Enhanced Controllability Through Vortex Manipulation on Fighter Aircraft at High Angles of Attack," AIAA Paper 86-2277, Aug. 1986.

[2]Malcolm, G. N., Ng, T. T., Lewis, L. C., and Murri, D. G., "Development of Non-Conventional Control Methods for High Angle of Attack Flight Using Vortex Manipulation," AIAA Paper 2192, July 1989.

[3]Malcolm, G. N., and Ng, T. T., "Forebody Vortex Control for Aerodynamic Control of Aircraft at High Angle of Attack," Society of Automotive Engineers Paper 892220, Sept. 1989.

[4]Moskovitz, C., Hall, R., and DeJarnette, F., "Experimental Investigation of a New Device to Control the Asymmetric Flowfield on Forebodies at Large Angles of Attack," AIAA Paper 90-0068, Jan. 1990.

[5]Rosen, B., and Davis, W., "Numerical Study of Asymmetric Air Injection to Control High Angle-of-Attack Forebody Vortices on the X-29 Aircraft," AIAA Paper 90-3004, Jan. 1990.

[6]Tavella, D. A., Schiff, L. B., and Cummings, R. M., "Pneumatic Vortical Flow Control at High Angles of Attack," AIAA Paper 90-0098, Jan. 1990.

[7]Ng, T. T., and Malcolm, G. N., "Aerodynamic Control Using Forebody Blowing and Suction," AIAA Paper 91-0619, Jan. 1991.

[8]Ng, T. T., and Malcolm, G. N., "Aerodynamic Control Using Forebody Strakes," AIAA Paper 91-0618, Jan. 1991.

[9]Ng, T. T., Suarez, C., and Malcolm, G. N., "Forebody Vortex Control with Miniature, Rotatable Nose-Boom Strakes," AIAA Paper 92-0022, Jan. 1992.

[10]Smith, B. C., and Ng, T. T., "Mechanical Control of Vortices on Different F-16 Forebodies Using Miniature Rotatable Strakes," AIAA Paper 94-0048, Jan. 1994.

Shape Sensitivity Analysis of Divergence Dynamic Pressure

Manoj Bhardwaj* and Rakesh K. Kapania†
Virginia Polytechnic Institute and State University, Blacksburg, Virginia 24061

Introduction

In the design of future aircraft, airframe flexibility is a concern from the strength, control, and performance requirements, which need both structural and aerodynamic sensitivity analysis capabilities. Structural sensitivity has been developed over the past two decades for sizing (thickness, cross-section properties) and shape (configuration) variables.[1] Although aerodynamic sensitivity has not existed until recently, a sensitivity does exist for aircraft in subcritical compressible flow,[2] which incorporates disturbances of thickness, camber, or twist distribution. Yates[3] has proposed a new approach that considers general geometry variations including planform for subsonic, sonic, and supersonic unsteady, nonplanar lifting surface theory.

Received May 6, 1993; revision received March 15, 1994; accepted for publication Jan. 15, 1995. Copyright © by M. Bhardwaj and R. K. Kapania. Published by the American Institute of Aeronautics and Astronautics, Inc., with permission.

*Graduate Research Assistant, Aerospace and Ocean Engineering. Student Member AIAA.

†Professor, Aerospace and Ocean Engineering. Associate Fellow AIAA.